Int. J Heat Mass Transfer Vol. 20, pp 93–106. Pergamon Press 1977. Printed in Great Britain

INFRARED FLAME RADIATION

R. O. BUCKIUS
Department of Mechanical and Industrial Engineering, University of Illinois at Urbana-Champaign, Urbana, IL 61801, U.S.A.

and

C. L. TIEN
Department of Mechanical Engineering, University of California, Berkeley, CA 94720, U.S.A.

(*Received* 8 *December* 1975 *and in revised form* 16 *June* 1976)

Abstract—Gaseous and particulate absorption for a non-homogeneous medium is considered both analytically and experimentally. A simple peak partial pressure and peak temperature scaling method applicable to combustion zones is successfully employed for non-homogeneous intensity calculations. Experimentally, natural convection controlled diffusion flame radiation is investigated. Spectral measurements of the radiance and transmittance are reported for polystyrene, Delrin, and Plexiglas fuels. The homogeneous gray model is shown to predict the experimental results reasonably well, yet is useful only when experimental data exist. The homogeneous nongray approximation is found to be inapplicable to highly non-homogeneous pathlengths. Non-homogeneous nongray calculations are shown to be accurate and with the peak partial pressure and peak temperature scaling method, simple calculations are possible from fundamental properties of the flames.

NOMENCLATURE

A_{ij}, total band absorptance for jth band of the ith species;
$\bar{c}$, concentration of particles;
C_2, Planck's second constant;
f_v, volume fraction of soot particles;
I, intensity;
I^-, intensity in the negative s direction;
k_v, absorption coefficient;
L, pathlength;
n, real part of refractive index;
$n\kappa$, complex part of refractive index;
$\bar{n}$, complex index of refraction equal to $n-in\kappa$;
P, pressure;
P_{ei}, equivalent broadening pressure of the ith species;
Q_{abs}, particle absorption efficiency;
r, particle radius;
s, distance along line of sight;
T, temperature;
X, mass pathlength.

Greek symbols

α_{ij}, integrated band intensity;
β_{ij}, π times the mean line width-to-spacing ratio;
ε, emissivity;
λ, wavelength;
ν, wave number;
ρ, solid phase density of soot;
ρ_i, density of ith absorber;
τ, transmissivity;
$\Psi^{(3)}$, Pentagamma function;
ω_{ij}, band width parameter.

Subscripts

b, blackbody;
CO_2, carbon dioxide;
H_2O, water vapor;
i, species;
j, band of specific species;
p, particle;
sc, scaled parameter;
ν, wave number.

Superscripts

$^-$, (overbars) average values.

INTRODUCTION

INFRARED radiation from flames constitutes an essential element in many engineering problems, particularly in fire, furnace, and rocket plume applications. Consideration must be given to a medium in which both gaseous and particulate species are important. A flame from hydrocarbon fuels is composed of many gaseous components, the most important for thermal radiation calculations are water vapor and carbon dioxide. This is due to their typically high concentrations coupled with the high temperatures that exist in flames. Small solid particles, called soot, are generated in flames due to the incomplete combustion of the fuel. The soot contribution to radiation calculations is quite important in many flame calculations.

Many experimental and analytical investigations of flame radiation have been reported. Total radiance measurements for arrays of turbulent and laminar diffusion flames have been reported by Markstein [1, 2]. The homogeneous gray model was used along

with experimental results to predict the radiative properties for the diffusion flames. Taylor and Foster [3] presented homogeneous gray model results for gaseous–particulate mixtures at various concentrations and temperatures. The gray coefficients were correlated from spectral homogeneous path calculations. Spectroscopic measurements for luminous flames are reported by Sato *et al.* [4], for furnace configurations burning both gaseous and liquid fuels. The results show the different effects of the concentration of soot to emission. A simple homogeneous nongray model approach has been employed by Felske and Tien [5] to analytically quantify the gaseous and soot contributions in flame radiation. Stull and Plass [6] and Siddall and McGrath [7] have presented results on homogeneous soot radiation. The optical constants as well as homogeneous emissivity calculations for soot have been presented by Dalzell and Sarofim [8]. General non-homogeneous nongray analysis is needed for flame radiation. Considering only radiating gases, several investigators [9–11] have reported very general analytical techniques for non-homogeneous nongray radiation calculations and have compared them with experimental results.

In this work, consideration is given to the intensity leaving a line of sight in which both gaseous and particulate absorption are important and particulate scattering can be neglected. Gaseous and particulate emission and absorption for non-homogeneous pathlengths are investigated analytically and experimentally. The homogeneous gray model, the homogeneous nongray model, and the general non-homogeneous nongray model are systematically developed and a simple scaling method applicable to non-homogeneous flames is presented. The experimental study is based on measurements of the spectral transmittance and radiance of flames of various solid plastic fuels. Solid plastic fuels are considered due to their importance in fire safety and since spectral radiation measurements for solid fuels appear to be lacking. The three analytical methods applied to the experimental results are discussed and compared.

ANALYSIS

The equation of transfer for a line of sight s through an absorbing and emitting medium which is in local thermodynamic equilibrium is

$$(\mathrm{d}I_\nu/\mathrm{d}s) + k_\nu I_\nu = k_\nu I_{b\nu} \tag{1}$$

where I_ν is the spectral intensity, $I_{b\nu}$ is the Planck blackbody intensity, k_ν is the spectral absorption coefficient and ν denotes wave number. Integration of equation (1) over all wave numbers and along the line of sight from the point $s = L$ to the observer at $s = 0$ yields

$$I^-(0) = \int_0^\infty \int_0^L I_{b\nu}(s) \exp\left(-\int_0^s k_\nu \,\mathrm{d}s'\right) k_\nu(s)\,\mathrm{d}s\,\mathrm{d}\nu. \tag{2}$$

A medium containing more than one component is characterized by the spectral absorption coefficient that is the sum of the spectral absorption coefficients of each species. With the transmissivity defined as

$$\tau_{\nu i}(s) = \exp\left(-\int_0^s k_\nu \,\mathrm{d}s'\right) \tag{3}$$

the transmissivity for a mixture of i components is

$$\tau_\nu(s) = \prod_i \tau_{\nu i}(s) \tag{4}$$

which is strictly valid only for monochromatic radiation although it is found to be true experimentally over finite spectral intervals [12]. The intensity in equation (2) becomes

$$I^-(0) = \int_0^\infty \int_0^L I_{b\nu}(s)\left(-\frac{\mathrm{d}\tau_\nu(s)}{\mathrm{d}s}\right)\mathrm{d}s\,\mathrm{d}\nu \tag{5}$$

where $\tau_\nu(s)$ can represent a mixture of components.

Homogeneous gray model

The absorption and emission of radiant energy by a mixture of gases and particles is a function of the concentration, temperature, and pathlength. The radiative transfer calculation for a line of sight is, therefore, dependent upon the variation of these parameters along the pathlength. This can result in very complicated computations for mixtures of many components. For simplification, the temperature and pressure are often taken as constants resulting in a homogeneous path approximation. Another major simplification in the analysis is achieved if it is assumed that one mean value of the absorption coefficient can account for all spectral variations. These two approximations yield the homogeneous gray model.

For the absorption coefficient which is not a function of wave number or pathlength, equation (5) becomes

$$I^-(0) = (\sigma T^4/\pi)[1 - \exp(-kL)] \tag{6}$$

where k is a total averaged absorption coefficient. The use of this homogeneous gray equation is dependent upon the prescription for k. Experimental measurements are a means of determining the mean coefficient. Results have been reported for various laminar and turbulent premixed flames [1] using both a single gray model term and a superposition of gray model terms. Experimental results presented in later sections are used to determine k for the natural convection controlled diffusion flames of plastic fuels.

Homogeneous nongray model

The intensity for a homogeneous path is obtained from equation (5) as

$$I^-(0) = \int_0^\infty I_{b\nu}[1 - \tau_\nu(L)]\,\mathrm{d}\nu. \tag{7}$$

The spectral variation of the transmissivity for an i.r. radiating gas is due to the vibrational–rotational bands. The spectral dependence can be evaluated for practical calculations by the wide band methods [13–16]. In particular, the exponential wide band model [13, 14] has been successfully employed for various combustion gases.

For a gaseous medium with a single vibrational–rotational band, the frequency dependence for a band

is restricted to a small interval as compared to the blackbody spectrum. For this reason, I_{bv} is removed from the integral in equation (7) and taken constant at the wavelength of the band head or center depending upon the type of band to give

$$I^-(0) = \overline{I_{bij}} A_{ij} \tag{8}$$

where the total band absorptance for the jth band of the ith species is

$$A_{ij} = \int_0^\infty [1-\tau_v(L)]\,dv. \tag{9}$$

Use of wide band prescriptions for the integrated band intensity α_{ij}, the band width parameter ω_{ij}, the mean line width-to-spacing ratio β_{ij}, and the equivalent broadening pressure P_{ei} in the transmissivity of equation (9) allows the total band absorptance to be determined for each gas band. The simple correlation of Tien and Lowder [16] is particularly convenient for the calculation of the total band absorptance. When two or more gases have bands in the same spectral interval, an overlap correction must be introduced. This factor has been considered by Penner and Varanasi [17] for water vapor and carbon dioxide mixtures. With equation (8), the total band absorptances, and the overlap correction factors, the intensity leaving a homogeneous mixture of gases can be evaluated. Before evaluation of the intensity leaving a mixture of both gases and particles is possible, a medium containing only particles must be considered.

Small particles present in a medium attenuate radiation continuously throughout the spectrum. For small particle absorption, using any size distribution, the governing equation for the absorption coefficient is given as [8, 18]

$$k_{vp} = \tfrac{3}{2}\frac{Q_{abs}}{2r} f_v = \frac{36\pi f_v}{\lambda} \frac{nn\kappa}{[n^2-(n\kappa)^2+2]^2+(2nn\kappa)^2} \tag{10}$$

where κ_{vp} is the particle absorption coefficient, r the particle radius, Q_{abs} the absorption efficiency, f_v the volume fraction of particles, and $\bar{n} = n - in\kappa$ the index of refraction. The actual wavelength variation indicated in equation (10) is dependent upon the variation of $\bar{n}$ for the specific particles. For soot particles that are contained in combustion systems, the values have been reported for different soots as a function of wavelength [8, 18]. The results show only a slight increase with wavelength and do not vary markedly for different soots. Also, the absorption coefficient is shown to be independent of temperature.

Using equation (10) in the transmissivity given in equation (3) results in

$$\tau_{vp}(s) = \exp\left(-\tfrac{3}{2}\frac{Q_{abs}}{2r}\int_0^s f_v\,ds'\right). \tag{11}$$

For a homogeneous path, f_v is a constant and the integral in equation (11) is $f_v s$. The total intensity is obtained by assuming the inverse wavelength behavior of the absorption coefficient since the optical constants are only weak functions of wavelength. Therefore, for a homogeneous path

$$I_p^-(0) = \frac{\sigma T^4}{\pi}\left[1-\frac{15}{\pi^4}\Psi^{(3)}\left(1-\tfrac{3}{2}\frac{Q_{abs}\lambda}{2r}\frac{f_v TL}{C_2}\right)\right] \tag{12}$$

where $\Psi^{(3)}$ is the pentagamma function and C_2 is Planck's second constant. This result gives the intensity for a particulate medium in terms of the particle's properties, temperature, and pathlength. This can also be used to determine the temperature of the homogeneous path if f_v, Q_{abs}, and L are known.

If the medium is composed of both particles and gases, the overlapping spectra must be analyzed. Particulate emission and absorption is continuous and is essentially constant over the banded gas regions. Therefore, the particle transmissivity can be removed from integrals over gas bands and evaluated at the band center or head. The governing equation for the total intensity is

$$I^-(0) = \int_0^\infty I_{bv}(1-\tau_{vp})\,dv + \sum_{ij}\bar{\tau}_{vp_{ij}} I_{bv_{ij}} A_{ij} \tag{13}$$

where A_{ij} accounts for the overlap of species with one another and τ_{vp} is the transmissivity of the particles. The first term denotes the intensity resulting from particulates and is given by equation (12). The second term denotes the gaseous contribution that is transmitted through the particles. This is the result for the intensity leaving a homogeneous path containing gases and particles. The applicability of this result is dependent upon the degree of homogeneity present in the system.

Non-homogeneous nongray model

The most complete method to determine the intensity from a general pathlength is to incorporate the variations in temperature and pressure. The analysis needed is, therefore, more complicated, and more detailed information is required. The resulting expressions are used for pathlengths that have large variations in temperature and pressure where the homogeneous nongray model is no longer valid.

The general non-homogeneous intensity at $s = 0$ is given in equation (5). Similar to equation (13) for a homogeneous nongray path, the non-homogeneous nongray model for a mixture of particles and gases is given as

$$I^-(0) = \int_0^\infty \int_0^L I_{bv}\frac{d}{ds}[1-\tau_{vp}(s)]\,ds\,dv + \int_0^L \overline{I_{bv}}\frac{d}{ds}\left\{\overline{\tau_p(s)}\int_0^\infty [1-\tau_{v\theta}(s)]\,dv\right\}ds. \tag{14}$$

The definition of the total band absorptance given in equation (9) pertains only to a homogeneous path. It is desirable to use this same expression for a non-homogeneous path defining scaled values for the parameters α_{ij}, ω_{ij}, $\beta_{ij} P_{ei}$, and $\rho_i s$. Therefore, introducing equation (9) into equation (14) gives

$$I^-(0) = \int_0^\infty \int_0^L I_{bv}\frac{d}{ds}[1-\tau_{vp}(s)]\,ds\,dv + \int_0^L \sum_{ij}\overline{I_{bv_{ij}}}\frac{d}{ds}[\overline{\tau_{vp_{ij}}} A_{ij}]\,ds \tag{15}$$

where the overlap correction is introduced into A_{ij}. The terms of equation (15) are interpreted in a similar manner to the homogeneous result [equation (13)] except that all quantities are now pathlength dependent. This is the general governing expression for the non-homogeneous nongray model.

It remains to determine the scaled values of the wide band parameters for use in the homogeneous total band absorptance. A highly simplified method [11] which predicts non-homogeneous total band absorptances nearly identical to the more general method of Chan and Tien [19] uses average values for T and P in the scaled parameters. This work gives

$$\alpha_{sc} = \alpha(\bar{T});\ \omega_{sc} = \omega(\bar{T});\ (\beta P_e)_{sc} = \beta P_e(\bar{T}, \bar{P});\ X_{sc} = \bar{\rho} s \tag{16}$$

where the subscript sc denotes a scaled quantity for use in the homogeneous total band absorptances to give the non-homogeneous result and X is the mass pathlength for the species considered. The average values are given by

$$\bar{\sigma} = \frac{1}{s}\int_0^s \sigma \, ds'. \tag{17}$$

The use of any of the scaling techniques requires detailed pathlength information about the variation of the partial pressure and temperature. In most cases, this information is unavailable or impossible to predict analytically. It is highly desirable to simplify the calculation procedure so that radiation calculations can be made from the least amount of detailed information within the accuracy of the wide band model. Special attention is given to partial pressure distributions that follow the temperature distributions which occur in the high temperature combustion zones. It has been found that only peak values of the partial pressures and temperatures need be used in the scaled quantities of the total band absorptance for use in calculating the non-homogeneous intensity. This is a result of the importance of the high temperature regions for radiation calculations. Also, calculations show that the overlap correction factor can be neglected within an accuracy of 9% for large pathlengths (200 cm) and within a small fraction of 1% for short pathlengths (5 cm). Thus, this scaling procedure does not require the knowledge of the partial pressure distribution and only peak partial pressures need to be estimated.

Non-homogeneous intensity calculations are presented for 12 mixtures indicated in Figs. 1–3. The intensity calculations have been performed using the scaling method indicated in equations (16) and (17) and the peak method proposed. The Tien–Lowder expression [16] was used to determine the total band absorptances coupled with the overlap correction [17]. The individual band intensity, total non-homogeneous intensity, and correction factor intensity are presented in Table 1.

Good agreement is achieved for the non-homogeneous intensity considering the simplicity of the proposed method and the accuracy of the wide band formulation. The agreement can be attributed to the

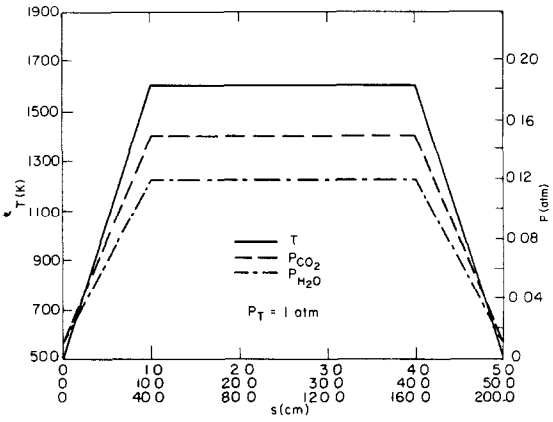

FIG. 1. Assumed non-homogeneous profiles: (three different pathlengths for each profile).

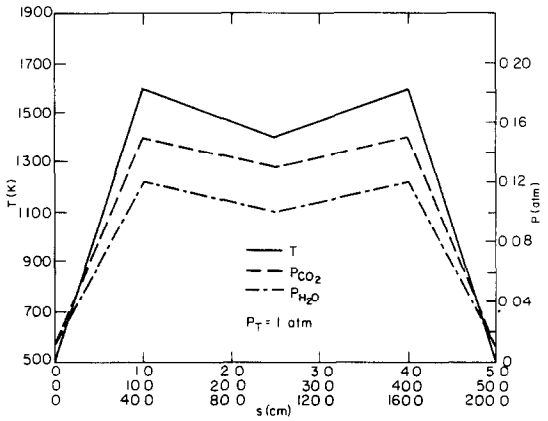

FIG. 2. Assumed non-homogeneous profiles: (three different pathlengths for each profile).

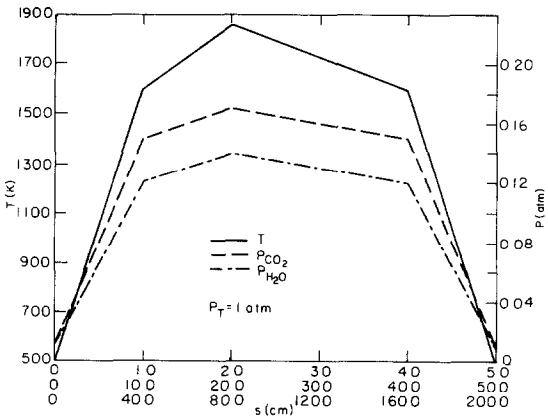

FIG. 3. Assumed non-homogeneous profiles: (three different pathlengths for each profile).

fact that the peak values predict the derivative of the total band absorptance quite reasonably. The values of the total band absorptance might not agree, yet the derivatives of total band absorptance, being more important to non-homogeneous calculations, do not differ appreciably. The case of the short pathlength calculations for each of the distributions is of specific interest. The maximum error that results for any single band intensity due to the peak scaling method is 8.5% and the error is generally less than 4%. These errors

Table 1. Peak Partial pressure and peak temperature scaling method

Figure	Pathlength (cm)		Intensities (W/cm^2) H_2O 2.7 μ Band	H_2O 6.3 μ Band	CO_2 2.7 μ Band	CO_2 4.3 μ Band	Overlap correction	Total intensity
1	5	Ref. [11]	0.0318	0.0369	0.0235	0.1789	0.0002	0.2709
		Peak values	0.0321	0.0381	0.0245	0.1713		0.2659
	50	Ref. [11]	0.2689	0.2545	0.1823	0.2758	0.0177	0.9639
		Peak values	0.2708	0.2630	0.1827	0.2195		0.9356
	200	Ref. [11]	0.6925	0.5380	0.3974	0.3015	0.1438	1.7855
		Peak values	0.6757	0.5255	0.3694	0.2100		1.7750
2	5	Ref. [11]	0.0258	0.0328	0.0188	0.1562	0.0002	0.2334
		Peak values	0.0266	0.0347	0.0204	0.1525		0.2342
	50	Ref. [11]	0.2170	0.2224	0.1462	0.2430	0.0152	0.8134
		Peak values	0.2245	0.2398	0.1524	0.1994		0.8159
	200	Ref. [11]	0.5576	0.4686	0.3230	0.2648	0.1214	1.4926
		Peak values	0.5640	0.4831	0.3079	0.1911		1.5454
3	5	Ref. [11]	0.0400	0.0417	0.0304	0.2108	0.0002	0.3227
		Peak values	0.0406	0.0433	0.0330	0.2061		0.3230
	50	Ref. [11]	0.3430	0.2958	0.2373	0.3264	0.0203	1.1821
		Peak values	0.3494	0.3152	0.2463	0.2680		1.1784
	200	Ref. [11]	0.8984	0.6350	0.5170	0.3594	0.1701	2.2397
		Peak values	0.8988	0.6497	0.4862	0.2559		2.2895

are all within the accuracy of the wide band formulation. This result is used for diffusion flames to determine the peak partial pressures for intensity calculations. The pathlength for each flame is less than 5 cm and thus the errors that result are small.

EXPERIMENTAL APPARATUS AND PROCEDURE

The experimental apparatus for determining the spectral radiance and transmittance of radiant energy is shown in Fig. 4. It consists of three major components: the source unit, the test chamber, and the detection unit. The source and detection units are essentially the same as described previously [20, 21]. The radiant energy is supplied by a globar which is heated electrically tp approximately 1470 K. The radiant beam from the globar is focused, chopped for identification, and collimated in the source unit. The exiting beam is directed through the test chamber and focused on the entrance of the detector.

The monochromator (Perkin–Elmer model 99) spectrally resolves the incident energy using a sodium chloride prism. The beam from the prism is then focused onto a thermocouple detector, converting the information to an electrical signal. The signal is sent to a lock-in voltmeter (Brower Laboratories model 131) and is plotted on a chart recorder. Calibration of the monochromator with respect to wavelength was necessary for all spectral measurements. Calibration with respect to energy was also necessary since radiance measurements were made in this study.

The burning samples were enclosed in the test chamber. Ventilation holes at the bottom and a suction fan at the top of the enclosure provided ambient air. Since natural diffusion of air to the flames was desired, only minimal air suction was used to remove the exhaust products. The samples inside the chamber were placed inside metal rings and on a grid that allowed passage of air around the samples. The samples were also spaced apart so that the presence of the other flames had a minor effect. The test section was completely isolated from the rest of the system.

Temperature distributions along the line of sight were obtained. The thermocouple used was formed from 76.2 μm (0.003 in) diameter platinum–13%

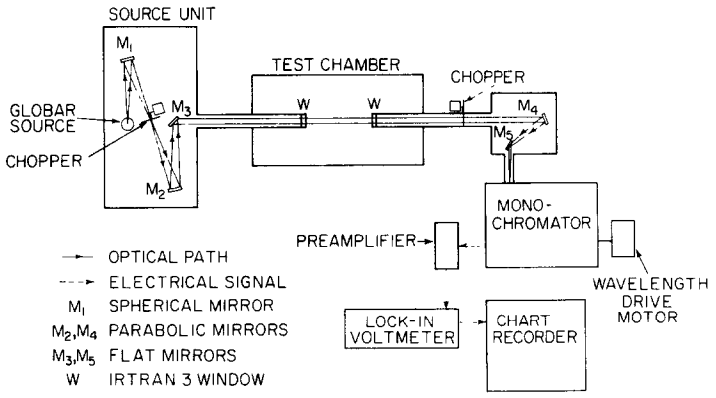

FIG. 4. The experimental system.

rhodium thermocouple wire to form a slightly larger bead [22]. To minimize catalytic effects, a yttrium oxide–beryllium oxide compound was applied to the thermocouple wire. A standard temperature correction was made by balancing the convective and radiative losses of the bead. The maximum correction was obtained by using the minimum convective losses. The emmissivity for the thermocouple coating obtained from measurements of Kent [23] is 0.7. The maximum correction is 120 K which is of the order of the fluctuations observed in the temperature measurements.

The radiance and transmittance for a specific free burning configuration depend upon the fuel and pathlength. The burning configuration investigated was a natural convection controlled diffusion flame that results from burning the flat surface of a 0.0762 m (3 in) dia plastic disk. Plexiglas (PMMA), Delrin, and polystyrene fuels were considered and the pathlength was varied from 2 to 5 flames as indicated in Fig. 5.

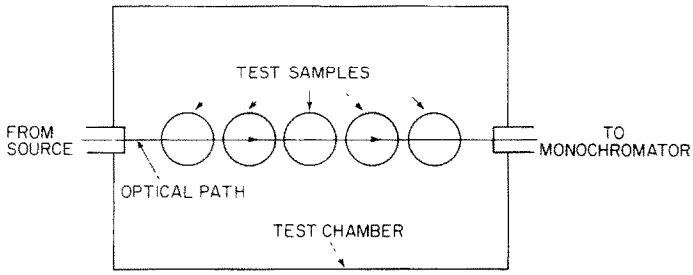

FIG. 5. The test configuration.

The samples were first ignited and allowed to reach a steady burning rate with the flame completely covering the plastic surface. Two sets of measurements for the radiance and transmittance were then made on each run. The radiance measurement used the test chamber exit chopper without the source and the transmittance measurement used the source unit chopper only. A run from 1.5 to 6.3 μm took approximately 5 min, and the sample had only burned about 0.0002 m below the original surface. Preliminary measurements were made at various heights above the plastic surface. These results showed similar spectra, only differing in magnitudes depending upon position. Therefore, the optical path was taken at 0.02 m above the plastic surface, approximately at the level of maximum radiance of the flames.

RESULTS AND DISCUSSION

The spectral radiance and transmittance for the three fuels are shown in Figs. 6–11. Each curve represents an average of at least two runs for the specified pathlength with the typical variation in the runs of approximately 10%. As noted in the figures, the qualitative features of the spectra are the same but the magnitudes are much different.

The results indicate that the gas bands of interest in the i.r. are those in the 4.3 and 2.7 μm regions. The larger 4.3 μm band is due to the presence of CO_2 and the smaller 2.7 μm overlapping band region is produced by both CO_2 and H_2O. The continuous spectrum is produced by the soot particles that are present. For the regions of the spectrum covered, yet not presented (1.6 μm $> \lambda >$ 5.2 μm), the behavior was found to be very smooth. These regions are considered to be a result of the continuous soot spectrum. An H_2O band exists in the 6.3 μm region but is very low and wide and was unrecognizable from the low globar spectrum in that region. The contribution of this band to the total intensity for the fuels investigated is less than 12.5%.

The radiance and transmittance for polystyrene are shown in Figs. 6 and 7. The spectra are dominated by the continuous soot emission and absorption. The soot contribution to the total radiance is approximately between 80 and 90%. The opposite behavior is observed in the Delrin spectrum shown in Figs. 8 and 9. The emission from the gas is dominant. The CO_2 fundamental band at 4.3 μm contributes more than one-half of the total radiance and the soot radiance contributes only a maximum of 15%. The radiance and transmittance of PMMA are presented in Figs. 10 and 11. The spectra show comparable emission for the soot and the gas. Therefore, from the standpoint of heat-transfer calculations in flames from solid plastic fuels, all the possible radiation characteristics are covered by the samples studied. Measurements are presented for plastics with dominant soot radiation as well as with dominant gas radiation.

The total radiance and transmittance are given in Table 2. The total transmittance is the transmitted energy integrated over all wavelengths divided by the

Table 2. Total radiance and transmittance

	Radiance (W/cm²-str)				Transmittance			
No. of flames	5	4	3	2	5	4	3	2
Polystyrene	1.66	1.46	1.12	0.767	0.338	0.461	0.511	0.665
Plexiglas	1.15	1.03	0.799	0.528	0.826	0.870	0.895	0.934
Delrin	0.624	0.547	0.468	0.376	0.848	0.878	0.882	0.918

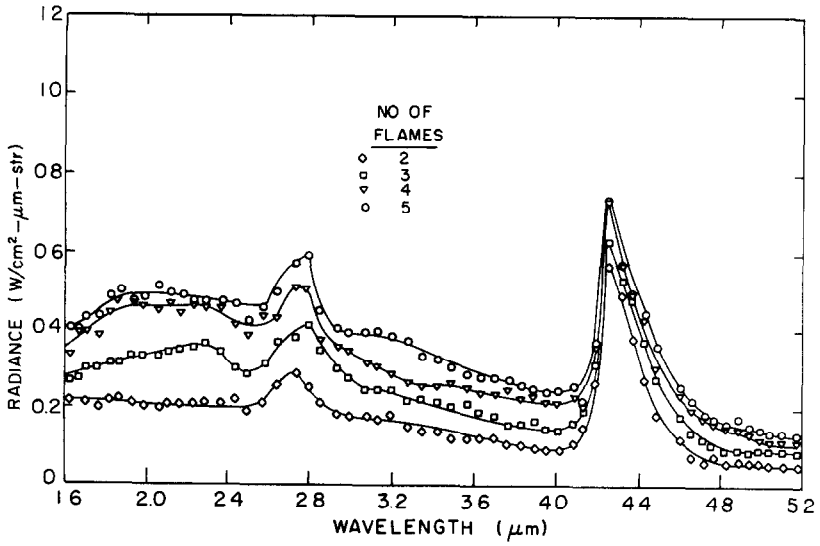

FIG. 6. Spectral radiance for polystyrene.

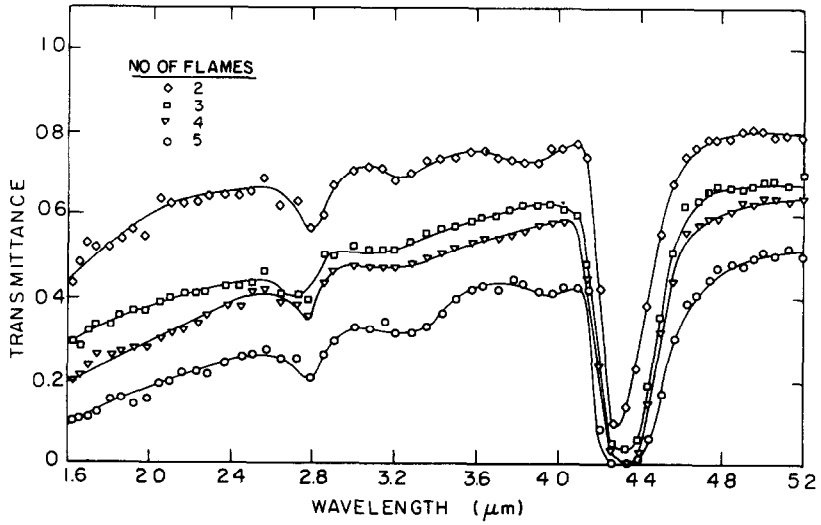

FIG. 7. Spectral transmittance for polystyrene.

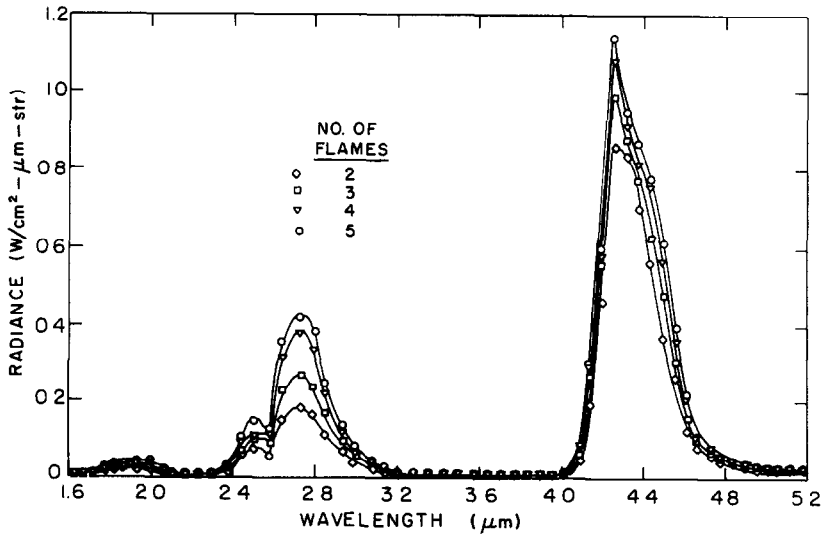

FIG. 8. Spectral radiance for Delrin.

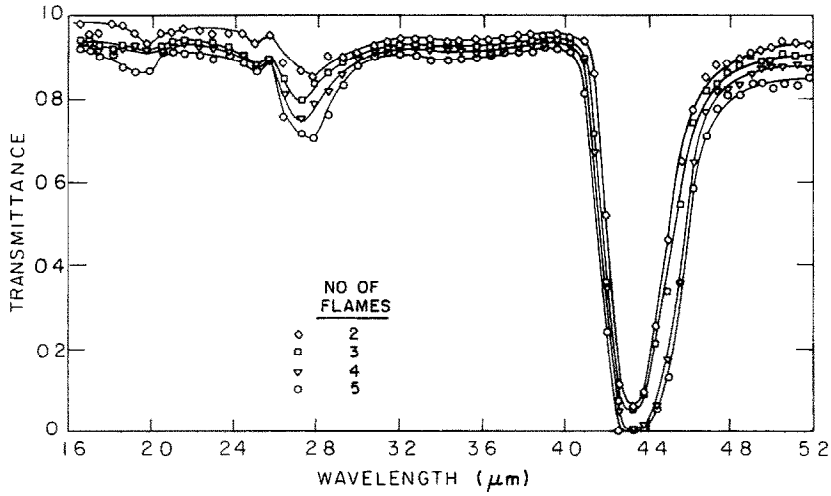

FIG. 9. Spectral transmittance for Delrin.

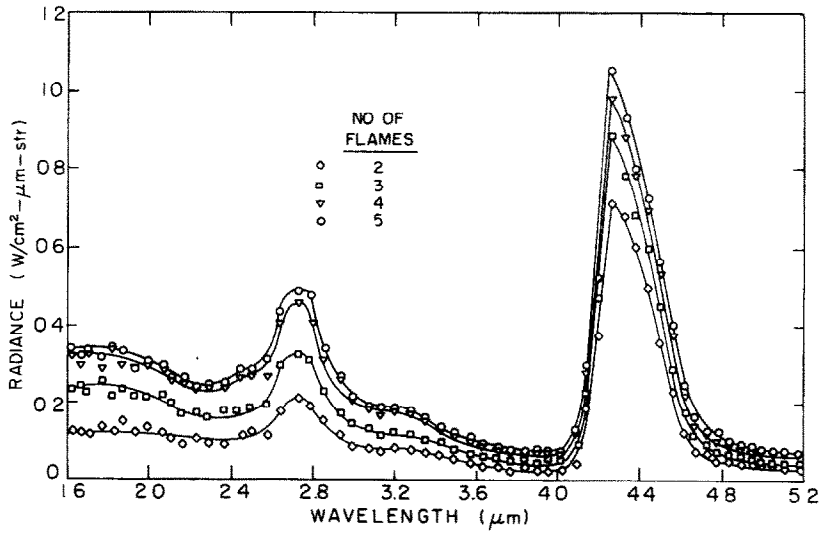

FIG. 10. Spectral radiance for Plexiglas.

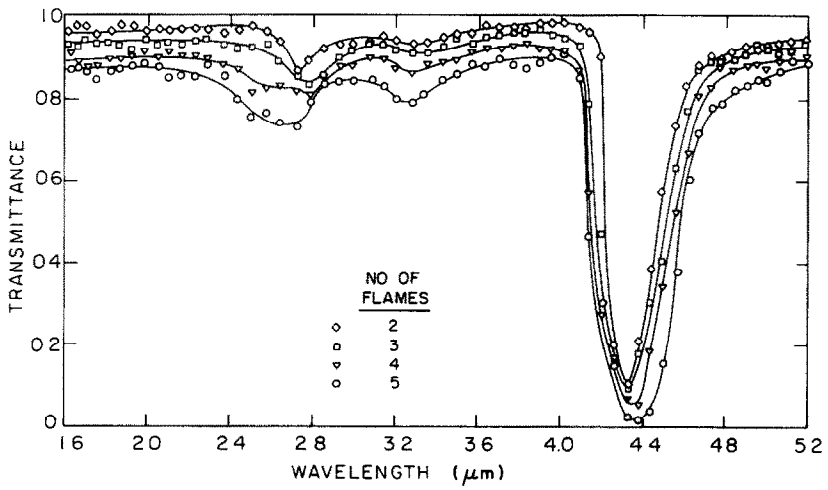

FIG. 11. Spectral transmittance for Plexiglas.

total incident energy. The incident energy from the globar was recorded for each run and, therefore, the total incident energy was found. Similar integrations for the transmitted energy result in the values presented in Table 2. The total radiance values were obtained by the same integration procedure.

The temperature distribution for each flame is presented in Fig. 12. The experimental measurements showed oscillation of the order of 100 K due to the unsteady nature of the flames. Therefore, the curves

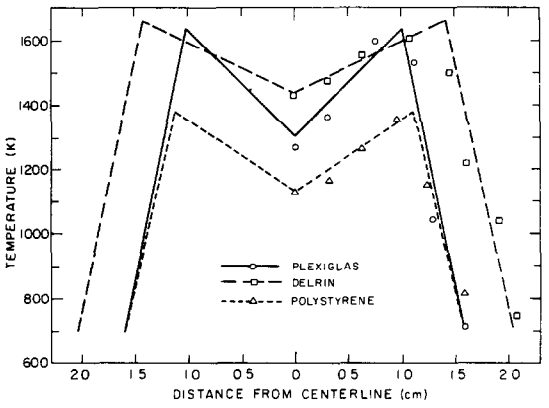

FIG. 12. The temperature distributions.

drawn through the data are only meant to be approximate representations for the temperature distribution. It is very interesting to compare the temperature distributions with the corresponding spectrum for each fuel. The average temperature tends to decrease with increasing soot radiance. The high soot radiative losses, coupled with more incomplete combustion (the fuels have similar adiabatic flame temperatures), could account for this behavior.

Attention is now directed to the analytical techniques developed previously to describe the experimental results. The aim is to assess the applicability of each analytical method to flame radiation calculations.

Homogeneous gray model

The homogeneous gray approximation results in a major simplification in radiation analysis. To apply this approximation, the total radiance and transmittance are needed. These results are given in Table 2 for each flame.

The mean absorption coefficient is obtained from the definition of the gray transmittance. This is presented in Table 3 for a single gray model. The values of the transmittance for both polystyrene and PMMA show a consistent scatter about the constant values given for the absorption coefficient. The Delrin result shows a distinct nongray trend, yet for the pathlengths considered, only a single absorption coefficient is adequate. For flames containing more soot (PMMA and polystyrene), a homogeneous gray model is more closely obeyed due to the smooth spectrum of the soot. The flames with the least soot show the largest nongray effect. This is also indicated in the work of Markstein [2].

To complete the homogeneous gray analysis, the equivalent temperature for the gray model is needed. From both the radiance and transmittance results and equation (6), the temperature is evaluated. The results are indicated in Table 3. The mean absorption coefficient determined above is then used to predict the emissivity of the flames and is presented in Fig. 13.

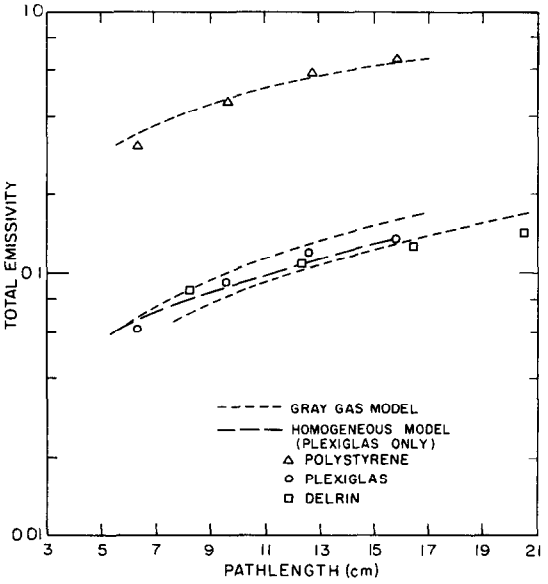

FIG. 13. Total emissivity vs pathlength.

Table 3. Homogeneous gray and nongray results

Gray model			Homogeneous model		
Polymer	T(K)	k(cm^{-1})	L(cm)	T(K)	I_s(W/cm^2 – str)
Polystyrene	1080	0.066	6.35	1055	0.632
			9.52	1080	0.957
			12.69	1100	1.280
			15.87	1105	1.490
Plexiglas	1420	0.011	6.35	1450	0.288
			9.52	1485	0.478
			12.69	1505	0.682
			15.87	1470	0.731
Delrin	1246	0.009	8.2	(Insufficient soot radiance)	
			12.3	(Insufficient soot radiance)	
			16.4	(Insufficient soot radiance)	
			20.5	900	0.092

Since the path is homogeneous, the emissivity is used and is defined as $\varepsilon = [I^-(0)]/[\sigma(T^4/\pi)]$. The maximum deviation of this calculation from the experimental points is 20%. The trend indicated by this analytical result differs slightly from the experimental points for the pathlengths investigated. The important point is that experimental data are needed to calculate the homogeneous gray model results.

Homogeneous nongray model

The soot radiance and transmittance are considered first since these results are needed throughout this section. The soot spectrum shown in Figs. 6–11 displays markedly different results depending upon the fuel. This is due to the different molecular compositions of each plastic and also to any differences that occur in the flow configurations and combustion of each fuel. Experimental findings have indicated that the optical properties are quite similar for most hydrocarbon soots [8, 18]. The densities of various soots have also been found to be relatively constant [24]. Therefore, the main difference in the soot spectra can be attributed to the concentration and temperature distribution for the pathlength.

The transmittance for the pathlength is obtained from equation (3) as

$$\tau(s) = \exp\left\{-L\left[\left(\int_0^L k_\lambda \, ds\right)\Big/ L\right]\right\}$$

where the quantity in brackets is defined as the average absorption coefficient for the soot. The soot contribution is obtained from the transmittance spectra in the regions between the banded gas spectra given in Figs. 7, 9, and 11. These results have been plotted in Fig. 14 with the error bars denoting the differences observed for the various pathlengths.

The important result from this plot is the inverse wavelength variation of the average soot absorption coefficient. The Rayleigh limit of small particulate absorption is observed and scattering can be neglected. This has also been shown by other experimenters [7] under different burning configurations and for different fuels. The results for PMMA and Delrin are multiplied by 10.0 in this figure and are much smaller than the polystyrene result. Note that a very limited number of points are indicated for the Delrin. This is due to the fact that the transmittance data show very little absorption by the soot. Consequently, any globar intensity variation results in uncertainty for the soot transmittance measurement.

For a homogeneous path the average soot absorption coefficient plotted in Fig. 14 becomes the soot absorption coefficient, since $k_{\lambda,p}$ is not a function of pathlength. Equation (11) is used to determine the volume fraction of soot for the homogeneous path once the properties of the soot are known. The results of Dalzell and Sarofim [8] indicate that a reasonable assumption is $n-1 = n\kappa$ for the i.r. Taking the optical properties as constants at their values in the near i.r. yields $n-1 = n\kappa = 1.0$, and the solid phase density is taken as $\rho = 1.65 \times 10^3 (\text{kg/m}^3)$ [24]. The resulting concentrations ($\bar{c}$) and volume fractions are presented in Table 4. As expected, the polystyrene flame has the largest soot concentration. This corresponds to the highest soot radiance of all the fuels. The other fuels show less soot concentration and thus less soot radiance.

The temperature of the soot is obtained by the use of equation (12). The values for Q_{abs}, f_v, and L are all known from the previous assumptions. The soot radiance and the blackbody function are continuous in wavelength; therefore, the soot spectra can be extended smoothly through the gas band regions. The soot radiance is then integrated and presented in Table 3.

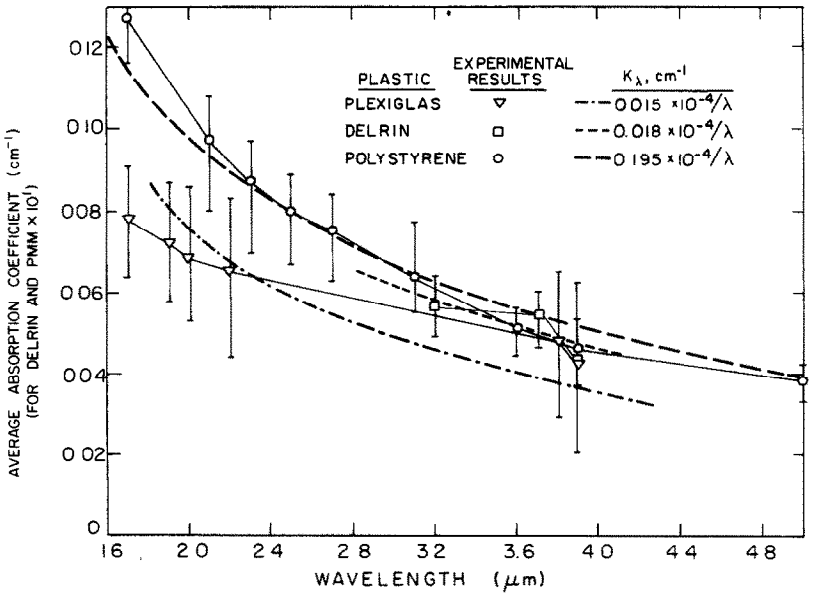

FIG. 14. Spectral absorption coefficient for soot.

Table 4. Homogeneous nongray soot results

Polymer	$k_\lambda(\text{cm}^{-1})$	f_v	$\bar{c}(\text{kg/m}^3)$
Polystyrene	$0.195 \times 10^{-4}/\lambda$	3.54×10^{-6}	5.83×10^{-3}
Plexiglas	$0.015 \times 10^{-4}/\lambda$	2.72×10^{-7}	4.49×10^{-4}
Delrin	$0.018 \times 10^{-4}/\lambda$	3.99×10^{-7}	6.58×10^{-4}

Note that the emission from the Delrin flame is so low that the only result shown is given for five flames. By a trial-and-error procedure, the soot temperature was obtained and is also shown in Table 3.

The results for the soot temperature show a tendency to increase with an increasing number of flames. This might be attributed to the non-independence of the flames. An equally probable explanation is the non-homogeneous effect. With an increasing number of flames, there is an increase in the number of low temperature regions within the pathlength. These low temperature flame regions tend to diminish the intensity leaving the path. Thus, when the homogeneous path assumption is imposed, the non-homogeneous cold regions are averaged into the pathlength. This is approximated as a homogeneous path and the resulting temperature must be larger.

The soot results above have determined the soot concentration, temperature, and transmittance for a homogeneous path. The homogeneous nongray model is then able to predict the gas properties. From the radiance measurements, the spectral gas band spectra can be obtained. This is integrated over each band to obtain the total radiance. Since the temperature is assumed to be a constant and known from the soot results, the total band absorptance is determined. The partial pressure of the gas specie is then determined from the total band absorptance.

A simple iteration scheme was used to evaluate the partial pressures of CO_2 and H_2O. The CO_2 partial pressure was evaluated from the 4.3 μm band since this band contributed the largest band radiance. The partial pressure of H_2O was then obtained from the 2.7 μm region. The overlap correction was evaluated [17] and all total band absorptances were evaluated using the Tien–Lowder correlation. The results for PMMA are $P_{H_2O} = 0.02\,\text{atm}$ and $P_{CO_2} = 0.17\,\text{atm}$. The homogeneous nongray calculation using equation (13) with these partial pressures and the average homogeneous temperature from Table 3 is shown in Fig. 13. The maximum deviation of the above homogeneous nongray calculation from the experimental results is 11.5%. This same procedure was applied to the polystyrene and Delrin flames. The results were not physically realistic. For the case of polystyrene, the soot domination resulted in gas partial pressures that were either too large or too small ($P_{CO_2} \to 1.0$, $P_{H_2O} \to 0.0$). This was also seen in the Delrin case since the soot radiance and, therefore, the soot temperature were too low. The non-homogeneous paths have greatly affected these predicted results.

The fact that the homogeneous path is not generally applicable to the flames investigated can be explained from the temperature distributions shown in Fig. 12. The pathlength is highly non-isothermal and for many flames this nonisothermal effect is increased. Also note that soot is formed from incomplete combustion and, therefore, would have high concentrations in the fuel-rich core of the flame. Thus, non-homogeneous concentration distributions also exist. The highly non-homogeneous distributions suggest that the homogeneous path approximation might not be valid.

The predictions of the homogeneous gray model and homogeneous nongray model (for PMMA) show good results in comparison with experimental results for the pathlengths considered. Since the experimental data are used to predict the needed information, this is not unexpected. However, two very important points are evident from the homogeneous gray and nongray approximations. The first is that even though the homogeneous gray model results in good predictions for the experimental data, the only method to predict the needed information (homogeneous temperature and mean absorption coefficient) accurately is from the experimental results. This excludes the possibility of predicting flame radiation from fundamental fuel and flame properties. On the other hand, the homogeneous approximation predicts the flame radiation from fundamental information. This approximate theory can be very useful for a system that is known to be approximately homogeneous. The homogeneous analysis cannot be applied to any general non-homogeneous pathlength. This suggests the necessity to investigate the more accurate non-homogeneous nongray analysis.

Non-homogeneous nongray model

The flame pathlength is known to be highly non-homogeneous. Each flame exhibits a colder region in the core where appreciable concentrations of H_2O, CO_2, and soot are expected. An increase in the number of flames increases the non-homogeneous effects. Therefore, a complete non-homogeneous nongray calculation is needed. The computation is more accurate but to obtain this accuracy more detailed information is necessary.

All measurements were made at a pathlength above the fuel surface which contained two combustion zones per flame. From simple combustion ideas, it is expected that peak partial pressures are to occur in the high temperature regions and decrease in concentration toward the center of the flame. Soot is expected to exist predominantly in the core of the flame due to insufficient oxidant to burn the fuel completely, especially in the lower portions of the flame where the soot has not escaped into the surroundings.

Total soot radiance given in Table 3 is used to determine the volume fraction of soot. Soot is assumed to be distributed homogeneously in the center of the flame. The length of this homogeneous core path is taken to be the distance between the flame peak temperature regions. The volume fraction of soot is then found using the temperature distribution, core length, and experimental soot radiance in equations (10), (11) and (5). The values for f_v and core length are given in

Table 5. Non-homogeneous nongray model results

Polymer	Volume fraction	Core length (cm)	P_{CO_2}(atm)	P_{H_2O}(atm)
Polystyrene	1.85×10^{-6}	2.22	0.11	0.05
Plexiglas	3.7×10^{-7}	2.22	0.22	0.06
Delrin	3.0×10^{-8}	2.87	0.18	0.06

Table 5. The average soot extinction coefficient defined previously from the transmittance is also applicable for a non-homogeneous path. Comparison with values in Table 5 is quite reasonable for PMMA and polystyrene. For Delrin, the average soot extinction coefficient given by the transmittance measurement is much larger than the value obtained from the soot radiance. This discrepancy, discussed earlier in relation to Fig. 14, is attributed to the uncertainty in the Delrin soot transmittance.

Gas properties are then evaluated since the soot distribution is known. The method is similar to the homogeneous nongray method now using the non-homogeneous results. On a spectral basis, the quantity

$$\int_0^L I_{bv} \frac{\mathrm{d}}{\mathrm{d}s} \{\tau_{v,p}(s)[1-\tau_{vg}(s)]\}\,\mathrm{d}s$$

is obtained from the difference of the experimental spectral radiance and the spectral soot radiance. This is integrated over the banded regions to obtain the band quantities. Equation (15) is then used to evaluate the partial pressures from the experimental radiance and temperature measurements. The peak value scaling method was employed throughout the non-homogeneous computations. It is exceedingly useful since only the temperature distribution needed to be known. Comparisons between the non-homogeneous intensity calculated from scaling the temperature and an assumed partial pressure distribution and the non-homogeneous intensity calculated from the peak value scaling method were made for all the calculations. The differences were very small as indicated by the results in the analytical section. The peak partial pressures are presented in Table 5 and their radiance predictions are shown in Fig. 15.

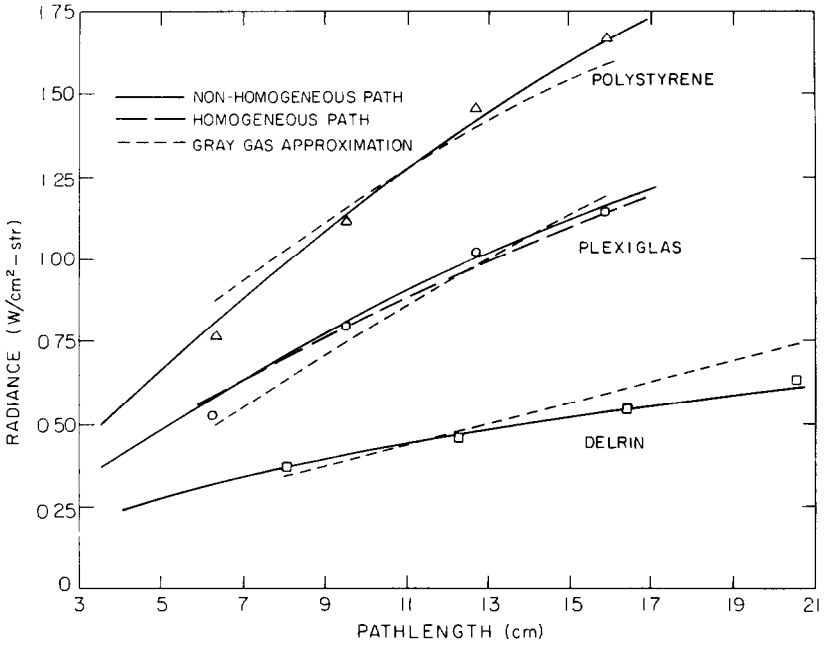

FIG. 15. Radiance vs pathlength.

For comparison with the above partial pressures, values of the partial pressures of CO_2 and H_2O that would result from a single-step combustion process for each fuel are shown in Table 6. These are assumed to be the only combustion products produced from the complete combustion of the fuels with air. Since this is not truly the situation, it is expected to give an estimate of the maximum values for the peak temperature regions. The wide band method above is not in-

Table 6. Stoichiometric partial pressures

Polymer	P_{CO_2}(atm)	P_{H_2O}(atm)
Polystyrene, $(C_8H_8)_n$	0.16	0.08
Plexiglas, $(C_5H_8O_2)_n$	0.16	0.13
Delrin, $(CH_2O)_n$	0.17	0.17

tended to predict the partial pressures exactly but rather to verify the non-homogeneous theory. Therefore, the partial pressures presented in Tables 5 and 6 are in reasonable agreement.

The non-homogeneous nongray radiance calculations show very good agreement with the experimental data. The maximum deviation of these calculations from the experimental results is 12%. In all calculations presented, the 6.3 μm band of H_2O has not been included since the experimental results did not account for it. The maximum contribution of this band is 12.5% as determined from the theoretical calculations. The non-homogeneous pathlength dependence is in good agreement with the experiment.

CONCLUSIONS

For a non-homogeneous mixture of gaseous species, the peak partial pressure and peak temperature scaling method is found to be accurate. The peak temperature regions for a general pathlength are very important in radiation calculations. For partial pressure distributions that follow the temperature distribution, as in combustion zones, the partial pressure distributions need not be known. Only peak partial pressures need to be used to determine the non-homogeneous intensity. Since in many systems the gas concentration distribution is not known or difficult to predict analytically, this method is very useful.

Spectral radiance and transmittance measurements for Plexiglas, Delrin, and polystyrene flames are presented. The importance of H_2O, CO_2, and soot is shown in these results. The polystyrene fuel exhibits dominant soot radiance and also the lowest mean temperature. The opposite behavior is seen in the case of Delrin where the gas band emission is the most important and the flame has the largest mean temperature. The Plexiglas fuel shows intermediate results.

All the analytical calculations are presented in Fig. 15. The first point to notice is the pathlength variation predicted by each of the models. Both the homogeneous and non-homogeneous nongray models predict the pathlength dependence very accurately for the PMMA. The non-homogeneous predictions of the other flames are also quite good. In comparison, the homogeneous gray model shows a differing trend from the data even though the actual deviation from the experimental data is small (maximum of 20%). This is a result of the fact that the problem is not gray or homogeneous and the governing equation is not strictly applicable. The other important point concerns the information that is needed to make analytical predictions. The homogeneous gray model needs experimental data to give accurate predictions and, at this point, it is impossible to obtain analytical representations from fundamental properties. The homogeneous and non-homogeneous nongray models use fundamental data of the flame to predict the radiation. The homogeneous nongray model is fairly simple and can be used if the pathlength is known to be approximately homogeneous but cannot be applied to any general problem. The non-homogeneous nongray model applies to all pathlengths but is more complicated making more detailed information necessary. The peak value scaling simplifies the calculations making non-homogeneous computations practical for flame combustion zones.

Acknowledgement—This research was supported by the National Science Foundation in the Fire Research Program, Research Applied to National Needs (RANN), through Grant No. GI-43.

REFERENCES

1. G. H. Markstein, Radiative energy transfer from turbulent diffusion flames, ASME Paper No. 75-HT-7, Heat Transfer Conference (1975).
2. G. H. Markstein, Radiative energy transfer from gaseous diffusion flames, 15th Combustion Symposium (1974).
3. P. B. Taylor and P. J. Foster, The total emissivities of luminous and non-luminous flames, *Int. J. Heat Mass Transfer* **17**, 1591–1605 (1974).
4. T. Sato, T. Kumitomo, S. Yoshii and T. Hashimoto, On the monochromatic distribution of the radiation from the luminous flame, *Bull. Japan. Soc. Mech. Engrs* **12**, 1135–1143 (1969).
5. J. D. Felske and C. L. Tien, Calculation of the emissivity of luminous flames, *Combust. Sci. Technol.* **7**, 25–31 (1973).
6. V. R. Stull and G. N. Plass, Emissivity of dispersed carbon particles, *J. Opt. Soc. Am.* **50**(2), 121–129 (1960).
7. R. G. Siddall and I. A. McGrath, The emissivity of luminous flames, in *Ninth Symposium (International) on Combustion*, pp. 102–110. Academic Press, New York (1963).
8. W. H. Dalzell and A. F. Sarofim, Optical constants of soot and their applications to heat-flux calculations, *J. Heat Transfer* **91**, 100–104 (1969).
9. C. B. Ludwig, W. Malkmus, J. E. Reardon and J. A. L. Thomson, *Handbook of Infrared Radiation from Combustion Gases*, National Aeronautics and Space Administration Sp-3080, Washington, D.C. (1973).
10. D. K. Edwards, L. K. Glassen, W. C. Hauser and J. S. Tuchscher, Radiation heat transfer in nonisothermal nongray gases, *J. Heat Transfer* **89**, 219–229 (1967).
11. J. D. Felske and C. L. Tien, Infrared radiation from non-homogeneous gas mixtures having overlapping bands, *J. Quantve Spectrosc. Radiat. Transfer* **14**, 35–48 (1974).
12. R. M. Goody, *Atmospheric Radiation· I. Theoretical Basis*. Oxford University Press, Oxford (1964).
13. D. K. Edwards and W. A. Menard, Comparison of models for correlation of total band absorption, *Appl. Optics* **3**, 621–625 (1964).
14. C. L. Tien, Thermal radiation properties of gases, *Advances in Heat Transfer*, Vol. 5, pp. 253–324. Academic Press, New York (1968).
15. D. K. Edwards and A. Balakrishnan, Thermal radiation by combustion gases, *Int J. Heat Mass Transfer* **16**, 25–40 (1973).
16. C. L. Tien and J. E. Lowder, A correlation for total band absorptance of radiating gases, *Int. J. Heat Mass Transfer* **9**, 698–701 (1966).
17. S S. Penner and P. Varanasi, Effect of (partial) overlapping of spectral lines on the total emissivity of H_2O–CO_2 mixture ($T \geqslant 800°K$), *J. Quantve Spectrosc. Radiat. Transfer* **6**, 181–192 (1966).
18. C. R. Howarth, P. J. Foster and M. W. Thring, The effect of temperature on the extinction of radiation by soot particles, *Third International Heat Transfer Conference*, Vol. 5, pp. 122–128. A.I.Ch.E., New York (1966).
19. S. H. Chan and C. L. Tien, Total band absorptance of nonisothermal infrared-radiating gases, *J. Quantve Spectrosc. Radiat. Transfer* **9**, 1261–1271 (1969).
20. C. L. Tien and W. H. Giedt, Experimental determination of infrared absorption of high-temperature gases, in *Advances in Thermophysical Properties at*

Extreme Temperatures and Pressure, edited by S. Gratsch. ASME, New York (1965).
21. M. M. Abu-Romia and C. L. Tien, Measurements and correlations of infrared radiation of CO at elevated temperatures. *J. Quantve Spectrosc. Radiat. Transfer* **6**, 143–167 (1966).
22. N. P. Cernansky, Formation of NO and NO_2 in a turbulent propane air diffusion flame, Ph.D. Thesis, University of California, Berkeley (1974).
23. J. Kent, Turbulent jet diffusion flames, Ph.D. Thesis, University of Sidney, Australia (1972).
24. P. J. Foster and C. R. Howarth, Optical constants of of carbon and coals in the infrared, *Carbon* **6**, 716–729 (1968).

RAYONNEMENT INFRAROUGE DES FLAMMES

Résumé—On considère, tant analytiquement qu'expérimentalement, l'absorption gazeuse et particulaire d'un milieu hétérogène. Une méthode à simple pic de pression partielle et de température, applicable aux zones de combustion, est employée avec succès pour le calcul du rayonnement. On considère expérimentalement le rayonnement des flammes de diffusion controlées par la convection naturelle. Des mesures spectrales d'émittance et de transmittance sont rapportées pour des combustibles polystyrène, Debrin et Plexiglass. Ce modèle du milieu gris et homogène estime raisonnablement les résultats expérimentaux. L'approximation du milieu non gris et homogène est inapplicable aux parcours fortement non homogènes. Les calculs pour un gaz non gris et hétérogène sont précis et avec la méthode du pic de pression partielle et de température, des calculs simples sont possibles pour les propriétés fondamentales des flammes.

INFRAROT-FLAMMENSTRAHLUNG

Zusammenfassung—Für ein inhomogenes Medium wird die Gas- und Partikelabsorption sowohl analytisch wie experimentell untersucht. Eine einfache, auf Verbrennungszonen anwendbare Methode zur Aufteilung der Spitzenwerte des Partialdrucks und der Temperatur wird erfolgreich zur Berechnung der inhomogenen Strahlungsintensität benutzt. Die Diffusionsflammenstrahlung bei natürlicher Konvektion wird experimentell untersucht. Spektralmessungen der Strahlung und Durchlässigkeit werden für die Brennstoffe Polystyrol, Delrin und Plexiglas aufgeführt. Es wird gezeigt, daß das Modell der homogenen, grauen Strahlung die Versuchswerte vernünftig wiedergibt, allerdings nur, wenn Meßwerte existieren. Die homogene, nichtgraue Näherung erweist sich als ungeeignet für große inhomogene Weglängen, während die inhomogene, nichtgraue Berechnung genaue Ergebnisse liefert. Mit Hilfe der Methode der Aufteilung der Spitzenwerte des Partialdruckes und der Temperatur können einfache Berechnungen unter Verwendung der grundlegenden Flammeneigenschaften durchgeführt werden.

ИНФРАКРАСНОЕ ИЗЛУЧЕНИЕ ПЛАМЕНИ

Аннотация — Проводится теоретическое и экспериментальное изучение поглощения газами и частицами в случае неоднородных сред. Для расчета неоднородной интенсивности успешно использовался простой метод масштабирования амплитудных значений парциального давления и температуры, применимый для зон горения. Экспериментально изучалось излучение диффузионного пламени при наличии конвекции. Приводятся данные спектральных измерений излучательной и пропускательной способности для полистирола, Дельрина и плексигласа. Показано, что с помощью гомогенной серой модели довольно хорошо обобщаются экспериментальные результаты, хотя она может быть полезной только при наличии экспериментальных данных. Отмечается, что аппроксимация для однородной серой среды не может быть применена в случае весьма неоднородных сред. Показано, что расчеты для несерой неоднородной среды довольно точны, а при использовании метода масштабирования амплитудных значений парциального давления и температуры возможны простые расчеты по основным свойствам пламени.